25. Nakatani K, Okuyama H, Shimahara Y, *et al.* Cytoglobin/STAP, its unique localization in splanchnic fibroblast-like cells and function in organ fibrogenesis. Lab Invest 2004;84:91–101.
26. Sugimoto H, Makino M, Sawai H, *et al.* Structural basis of human cytoglobin for ligand binding. J Mol Biol 2004;339:873–885.
27. Mathew J, Hines JE, Toole K, *et al.* Quantitative analysis of macrophages and perisinusoidal cells in primary biliary cirrhosis. Histopathology 1994;25:65–70.
28. Mouta Carreira C, Nasser SM, di Tomaso E, *et al.* LYVE-1 is not restricted to the lymph vessels: expression in normal liver blood sinusoids and down-regulation in human liver cancer and cirrhosis. Cancer Res 2001;61:8079–8084.
29. Bosselut N, Housset C, Marcelo P, *et al.* Distinct proteomic features of two fibrogenic liver cell populations: hepatic stellate cells and portal myofibroblasts. Proteomics 2010;10:1017–1028.
30. Gabbiani G, Majno G. Dupuytren's contracture: fibroblast contraction? An ultrastructural study. Am J Pathol 1972;66:131–146.
31. Darby I, Skalli O, Gabbiani G. Alpha-smooth muscle actin is transiently expressed by myofibroblasts during experimental wound healing. Lab Invest 1990;63:21–29.
32. Gabbiani G. The myofibroblast in wound healing and fibrocontractive diseases. J Pathol 2003;200:500–503.
33. Desmoulière A, Tuchweber B, Gabbiani G. Role of the myofibroblast differentiation during liver fibrosis. J Hepatol 1995;22(2 Suppl):61–64.
34. Niki T, Rombouts K, De Bleser P, *et al.* A histone deacetylase inhibitor, trichostatin A, suppresses myofibroblastic differentiation of rat hepatic stellate cells in primary culture. Hepatology 1999;29:858–867.
35. Wake K. Perisinusoidal stellate cells (fat-storing cells, interstitial cells, lipocytes), their related structure in and around the liver sinusoids, and vitamin A-storing cells in extrahepatic organs. Int Rev Cytol 1980;66:303–353.
36. Rege TA, Hagood JS. Thy-1 as a regulator of cell-cell and cell-matrix interactions in axon regeneration, apoptosis, adhesion, migration, cancer, and fibrosis. FASEB J 2006;20:1045–1054.
37. Kawai S, Enzan H, Hayashi Y, *et al.* Vinculin: a novel marker for quiescent and activated hepatic stellate cells in human and rat livers. Virchows Arch 2003;443:78–86.
38. Uyama N, Zhao L, Van Rossen E, *et al.* Hepatic stellate cells express synemin, a protein bridging intermediate filaments to focal adhesions. Gut 2006;55:1276–1289.
39. Wake K, Sato T. Intralobular heterogeneity of perisinusoidal stellate cells in porcine liver. Cell Tissue Res 1993;273:227–237.
40. Nakatani K, Seki S, Kawada N, *et al.* Expression of neural cell adhesion molecule (N-CAM) in perisinusoidal stellate cells of the human liver. Cell Tissue Res 1996;283:159–165.
41. Cassiman D, Libbrecht L, Desmet V, *et al.* Hepatic stellate cell/myofibroblast subpopulations in fibrotic human and rat livers. J Hepatol 2002;36:200–209.
42. Cassiman D, Denef C, Desmet VJ, *et al.* Human and rat hepatic stellate cells express neurotrophins and neurotrophin receptors. Hepatology 2001;33:148–158.
43. Li Y, Wang J, Asahina K. Mesothelial cells give rise to hepatic stellate cells and myofibroblasts via mesothelial-mesenchymal transition in liver injury. Proc Natl Acad Sci USA 2013;110:2324–2329.

JIR-2014-0096-ver9-Shimozono_1P
Type: research-article

JOURNAL OF INTERFERON & CYTOKINE RESEARCH
Volume 00, Number 00, 2015

DOI: 10.1089/jir.2014.0096

FULL MANUSCRIPT

AU1 ▶

Interferon-β Mediates Signaling Pathways Uniquely Regulated in Hepatic Stellate Cells and Attenuates the Progression of Hepatic Fibrosis in a Dietary Mouse Model

AU2 ▶

Rieko Shimozono,[1] Kazumi Nishimura,[1] Hideo Akiyama,[2] Saeko Funamoto,[3] Akiko Izawa,[1] Takafumi Sai,[1] Kana Kunita,[1] Mie Kainoh,[1] Tomohiko Suzuki,[1] and Norifumi Kawada[4]

The results of clinical and experimental studies suggest that type I interferons (IFNs) may have direct antifibrotic activity in addition to their antiviral properties. However, the mechanisms are still unclear; in particular, little is known about the antifibrotic activity of IFN-β and how its activity is distinct from that of IFN-α. Using DNA microarrays, we demonstrated that gene expression in TWNT-4 cells, an activated human hepatic stellate cell line, was remarkably altered by IFN-β more than by IFN-α. Integrated pathway enrichment analyses revealed that a variety of IFN-β–mediated signaling pathways are uniquely regulated in TWNT-4 cells, including those related to cell cycle and Toll-like receptor 4 (TLR4) signaling. To investigate the antifibrotic activity of IFN-β and the involvement of TLR4 signaling *in vivo*, we used mice fed a choline-deficient L-amino acid-defined diet as a model of nonalcoholic steatohepatitis-related hepatic fibrosis. In this model, the administration of IFN-β significantly attenuated augmentation of the area of liver fibrosis, with accompanying transcriptional downregulation of the TLR4 adaptor molecule MyD88. Our results provide important clues for understanding the mechanisms of the preferential antifibrotic activity of IFN-β and suggest that IFN-β itself, as well as being a modulator of its unique signaling pathway, may be a potential treatment for patients with hepatic fibrosis in a pathogenesis-independent manner.

Introduction

HEPATIC FIBROSIS IS A COMMON FEATURE of chronic liver diseases and can develop into cirrhosis, hepatic failure, and hepatocellular carcinoma (HCC). There are disparate causes that can lead to the development of hepatic fibrosis, but the main causes are chronic hepatitis C virus infection, autoimmune liver diseases, alcohol abuse, and nonalcoholic steatohepatitis (NASH). The hepatic stellate cells (HSCs) are primarily responsible for producing extracellular matrix in the injured liver (Friedman and others 1985; Gäbele and others 2003). Under physiologic conditions, the quiescent phenotypes of HSCs reside in the space of Disse outside sinusoids and store vitamin A when in the normal state. Following chronic injury, they undergo activation in response to inflammatory stimuli derived from injured hepatocytes and neighboring endothelial and Kupffer cells, and transdifferentiate into proliferative, fibrogenic, and contractile migrating myofibroblastic-like cells (Friedman 2000; Bataller and Brenner 2005).

Type I interferons (IFNs) constitute a pleiotropic cytokine family with antiviral, immunomodulatory, and antiproliferative effects. On the basis of their antiviral activity, IFN-β and IFN-α, classified as type I IFNs (Pestka and others 1987; Uzé and others 2007), have been widely used as therapeutic agents for viral eradication in patients with chronic viral hepatitis. Type I IFN therapy was found to suppress progressive fibrosis and prevent the subsequent occurrence of HCC in patients without virologic response (Almasio and others 2003; Soga and others 2005), indicating their therapeutic usefulness in preventing hepatic injury, fibrosis, and carcinogenesis. ◀ AU3

The differences in the antitumor effects of IFN-β and IFN-α have been thoroughly investigated, and there is a growing body of evidence showing that the antiproliferative effect of IFN-β on certain HCC cell lines is superior to that of IFN-α (Murata and others 2006; Damdinsuren and others 2007). Although IFN-β also has a preferential antiproliferative effect on HSCs (Shen and others 2002; Sekiya and others 2011), few studies have been published concerning the differences in the signaling pathways of IFN-β and IFN-α on HSC lines and the antifibrotic activity of IFN-β *in vivo*.

In this study, an immortalized and activated HSC line (Shibata and others 2003), TWNT-4, was shown to be a

[1]Pharmaceutical Research Laboratory and [2]New Projects Development Division, Toray Industries, Inc., Kamakura, Kanagawa, Japan.
[3]Department of Bio Research, Kamakura Techno-Science, Inc., Kamakura, Kanagawa, Japan.
[4]Department of Hepatology, Graduate School of Medicine, Osaka City University, Abeno, Osaka, Japan.

useful tool for analyzing the signaling pathway of IFN-β. As a result of DNA microarray analysis using TWNT-4 cells, we selected the appropriate experimental model of hepatic fibrosis and investigated the antifibrotic properties of IFN-β.

Materials and Methods

Interferons

Natural human IFN-α (Sumiferon; Dainippon Sumitomo Pharma) and natural human IFN-β (Feron; Toray Industries) were used in this experiment. Recombinant murine IFN-β derived from *Escherichia coli* were obtained from Kamakura Techno-Science.

Cell lines and cell culture

Human HSC line TWNT-4 cells, immortalized by retrovirally introducing human telomerase reverse transcriptase into LI 90 cells, an HSC line from the human liver mesenchymal tumor (Murakami and others 1995), were kindly provided by Dr. Naoya Kobayashi (Department of Surgery, Okayama University, Okayama, Japan, Present affiliation: Okayama Saidaiji Hospital, Okayama, Japan) with the permission of Okayama University (Okayama, Japan). The cells were maintained in Dulbecco's modified Eagle's medium containing 10% fetal bovine serum and 100 U/mL penicillin and 100 μg/mL streptomycin (Invitrogen). A human HCC-derived cell line, HuH-7 cells (JCRB0403) (Nakabayashi and others 1982), was obtained from the Japanese Collection of Research Bioresources and maintained in accordance with the provider's recommendation. All cells were incubated at 37°C in 5% CO_2 atmosphere.

Cell proliferation assay

The cells were plated at a density of 5×10^2 cells/well in a 96-well plate. The next day (day 0), the culture medium was replaced with a fresh one containing different concentrations of IFNs. On days 2, 4, 5, 7, and 11, viable cell count and cell viability values were determined by MTS methods using the CellTiter 96® AQueous One Solution Cell Proliferation Assay (Promega).

Flow cytometry

The TWNT-4 cells were serum starved for 21 h to synchronize the cells in the G0/G1 phase and then the medium was replaced with a fresh one containing IFNs (100 IU/mL) and serum. At 24 h after treatment, the cells were harvested by trypsinization, washed with phosphate-buffered saline (PBS), and fixed in ice-cold 70% ethanol. Following cell washing with PBS, cellular DNA was stained with 0.025 mg/mL propidium iodide (Life Technologies) in the presence of 100 μg/mL RNase A (Life Technologies). The fluorescence intensity of 10,000 cells was measured using a FACSCaliber flow cytometer (Becton Dickinson).

Western blot analysis

The TWNT-4 cells were treated with IFNs (100, 1,000 IU/mL). After treatment for 16 h, the cells were lysed with the RIPA lysis buffer containing protease and phosphatase inhibitors (Santa Cruz Biotechnology) and centrifuged (38,000 *g*, 10 min at 4°C) to remove insoluble material. Sample aliquots (20 μg of protein) were separated by 4–10% gradient SDS-PAGE and electrotransferred onto polyvinylidene difluoride membranes (Bio-Rad Laboratories). Nonspecific binding was blocked with Blocking One buffer (Nacalai Tesque) and incubated with the primary antibodies, anti-p21 (No. 2947; Cell Signaling Technology) and anti-actin (No. sc-1615; Santa Cruz Biotechnology). The membranes were washed with PBS with 0.1% Tween-20 and incubated with the secondary antibodies, alkaline phosphatase-labeled anti-rabbit IgG (Promega) and anti-goat IgG (Caltag Medsystems), respectively. The immunoreactive protein bands were visualized using a BCIP-NBT solution kit (Nacalai Tesque).

RNA extraction and quality check

The TWNT-4 and HuH-7 cells were treated with IFNs (100 IU/mL). After treatment for 4 h, total RNA was prepared from the cells using the RNeasy® Mini Kit (Qiagen). The RNA concentration and purity were assessed by UV absorbance determined using a NanoDrop Spectrophotometer ND-1000 (Nanodrop Technologies, Thermo Fisher Scientific). For microarrays, confirmation of the RNA quality was performed using a 2100 Bioanalyzer (Agilent Technologies).

DNA microarray

For the DNA microarray analysis, 1 μg of total RNA was amplified and labeled using an Amino Allyl MessageAmp™ II aRNA Amplification kit ((Applied Biosystems) in accordance with the manufacturer's instructions. Each sample of aRNA labeled with Cy3 or Cy5 was cohybridized with 3D-Gene™ Human Oligo chip 25k (Toray Industries) at 37°C for 16 h. After hybridization, each DNA chip was washed and dried. Hybridization signals were scanned using a ScanArray Express scanner (PerkinElmer) and processed by GenePix® Pro (Molecular Devices). The detected signals for each gene were scaled using the global normalization method (Cy3/Cy5 ratio median = 1). Integrated pathway enrichment analyses were performed using the knowledge-based canonical pathways in MetaCore™ (GeneGO).

Animals and in vivo experimental design

The animal experiments were conducted in accordance with the Guidelines for Animal Experiments, Research and Development Division, Toray Industries, Inc. Seven-week-old male C57BL6/N mice (Charles River Laboratories Japan) were randomly divided into 4 groups, that is, the naive group ($n = 3$), naive + IFN-β group ($n = 3$), choline-deficient L-amino acid-defined (CDAA) control group ($n = 5$), and CDAA + IFN-β group ($n = 5$). The mice in the CDAA control and CDAA + IFN-β groups were fed with a CDAA diet (Research Diets, Inc.) for 8 weeks. During the same period, the mice in the naive and naive + IFN-β groups were fed with the CRF-1 diet (Charles River Laboratories Japan). The mice in the naive + IFN-β and CDAA + IFN-β groups received IFN-β by tail vein injection from 4 weeks after feeding at a dose of 10^4 IU/body, thrice weekly (Monday, Wednesday, and Friday), for 4 weeks. Laparotomy and blood sampling were performed under isoflurane anesthesia 3 days after the last administration. After blood sampling, mice were euthanized by exsanguination under isoflurane anesthesia and the livers were immediately removed.

Histopathological examination

Formalin-fixed paraffin-embedded 2 μm-thick slices of liver were processed with hematoxylin and eosin stain and Sirius red stain using established methods. The NanoZoomer Digital Pathology System (Hamamatsu Photonics) was used to acquire digital high-resolution images through the 100× objectives. Image analysis was performed using Definiens XD software (Definiens). Three images per specimen were examined blindly and randomly and Sirius red-positive areas were quantified as the percentage of the fibrosis area.

Measurement of plasma transaminases

Plasma samples were obtained from the abdominal aorta using tubes containing lithium heparin and plasma separator (BD). Plasma alanine aminotransferase (ALT) and aspartate aminotransferase (AST) were measured using a DRI-CHEM system (Fujifilm).

Real-time quantitative polymerase chain reaction

Total RNA was extracted from each liver using the RNeasy Mini Kit (Qiagen) and translated into complementary DNA (cDNA) with High-Capacity cDNA Reverse Transcription kits (Applied Biosystems). Each cDNA was subjected to real-time quantitative polymerase chain reaction (qPCR) using the ABI-Prism 7000 and 7500 Sequence Detection System (Applied Biosystems) and amplified by the SYBR® Premix Ex Taq™ (TaKaRa Bio) reaction mixture utilizing gene-specific primers (Supplementary Table S1; Supplementary Data are available online at www.liebertpub.com/jir). The relative amount of each mRNA was determined using the $2^{-\Delta\Delta CT}$ method. The cycle threshold (Ct) values of each gene were corrected against values for the reference gene glyceraldehyde-3-phosphate dehydrogenase (GAPDH) (ΔCt) and normalized against the mean ΔCt of the naive group (ΔΔCt). ◀ ST1

Statistical analysis

In vivo quantitative data were analyzed by Wilcoxon's test. $P<0.05$ was considered statistically significant from the naive or CDAA control group.

Results

IFN-β inhibits proliferation of TWNT-4 cells more potently than IFN-α

To investigate the antifibrotic effects of type I IFNs on TWNT-4 cells, we first evaluated the effects of IFNs on the cell proliferation. While both IFN-β and IFN-α decreased cell proliferation at a concentration of 100 IU/mL, IFN-β was the more potent of the 2 (Fig. 1A, upper). A dose-response experiment also showed that IFN-β had a more potent antiproliferative effect on TWNT-4 cells than IFN-α (Fig. 1A, lower). This finding was based on the 50% ◀ F1

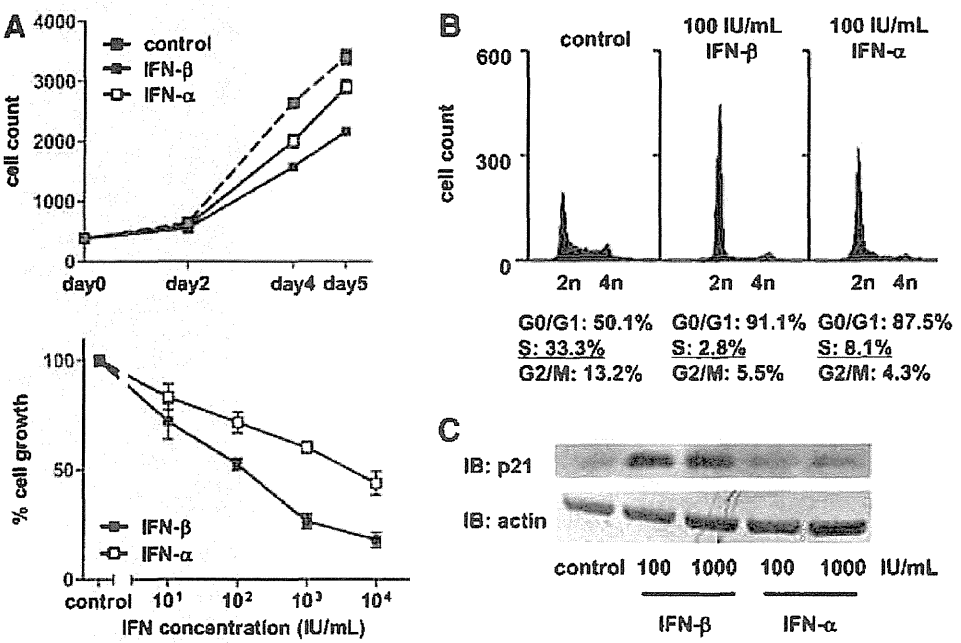

FIG. 1. IFN sensitivity profiling of TWNT-4 cells. (A) Cells were incubated with IFN-β or IFN-α (100 IU/mL) for 2–5 days (*upper*) or with IFN-β or IFN-α at the concentration of 10–10,000 IU/mL for 4 days (*lower*). Viable cell count was determined by MTS methods. Cell growth (*lower*) is shown as a percentage when the average cell number for control cells without IFNs was arbitrarily set to 100% and that for seeded cells on day 0 was arbitrarily set to 0%. The results shown represent the mean ± SD from triplicate-quintuplicate assays. (B) Cells synchronized in the G0/G1 phase were then incubated with IFN-β or IFN-α (100 IU/mL) for 24 h. The cell cycle was analyzed by flow cytometry. The *black* region indicates the histogram measured by flow cytometry, G0/G1 phase [*left*, diploid (2n) DNA content], G2/M phase [*right*, tetraploid (4n) DNA content], and S phase (between 2n and 4n), respectively. (C) Cells were incubated with IFN-β or IFN-α (100, 1,000 IU/mL) for 16 h. Cell lysates were subjected to IB with p21 antibody (*upper panels*). IB with actin antibody was used as a loading control (*lower panels*). (A–C) Control indicates nontreated cells. IB, immunoblot; IFN, interferon.

inhibitory concentration (IC_{50}) value, which calculated with linear extrapolation from the values above and below the inhibition threshold was 1.25×10^2 IU/mL for IFN-β and 4.21×10^3 IU/mL for IFN-α. This finding was confirmed in LI 90 cells, the parental cell line of TWNT-4 (Supplementary Fig. S1). SF1 ▶

Difference in the effect on G1 cell cycle arrest contributes to antiproliferative effect of IFNs in TWNT-4 cells

To analyze the mechanism of the antiproliferative effect of IFNs in TWNT-4 cells, the cell cycle distribution was determined. IFN-β treatment significantly decreased the S phase and the following G2/M phase population at 24 h after treatment; furthermore, the S phase population in the cells treated with IFN-β was smaller than in the cells treated with IFN-α at 24 h (Fig. 1B). We next tested for expression of a key regulator of the G1-S transition, p21/WAF1/CIP1 (Howe and others 1993), and observed increased expression of the p21 protein compared with the control preferentially induced by IFN-β, but not IFN-α (Fig. 1C). Together, these results indicate that IFN-β is superior to IFN-α in terms of induction of G1 arrest through an increase in p21, which is a mechanism that contributes to the antiproliferative effect of IFNs.

IFN-β alters gene expression profiles of TWNT-4 cells substantially more than IFN-α does, and in a different manner

Using a highly sensitive DNA chip, 3D-Gene (Nagino and others 2006), DNA microarray analyses were performed to characterize the type I IFN-induced gene alterations in HuH-7 and TWNT-4 cells and to compare differences between cell types. In HuH-7 cells, similar differential gene expression profiles were obtained in both IFN-β and IFN-α treatments (Fig. 2A, upper). In contrast, there was a striking difference in the number of genes altered between the IFN-β and IFN-α–treated TWNT-4 cells (Fig. 2A, lower), which indicates that there are various genes that are preferentially regulated by IFN-β in the cells. Genes that increased or decreased more than 1.5-fold were defined as having been altered. There were 2,083 and 1,947 differentially expressed genes in the IFN-β and IFN-α–treated HuH-7 cells, and ◀ F2

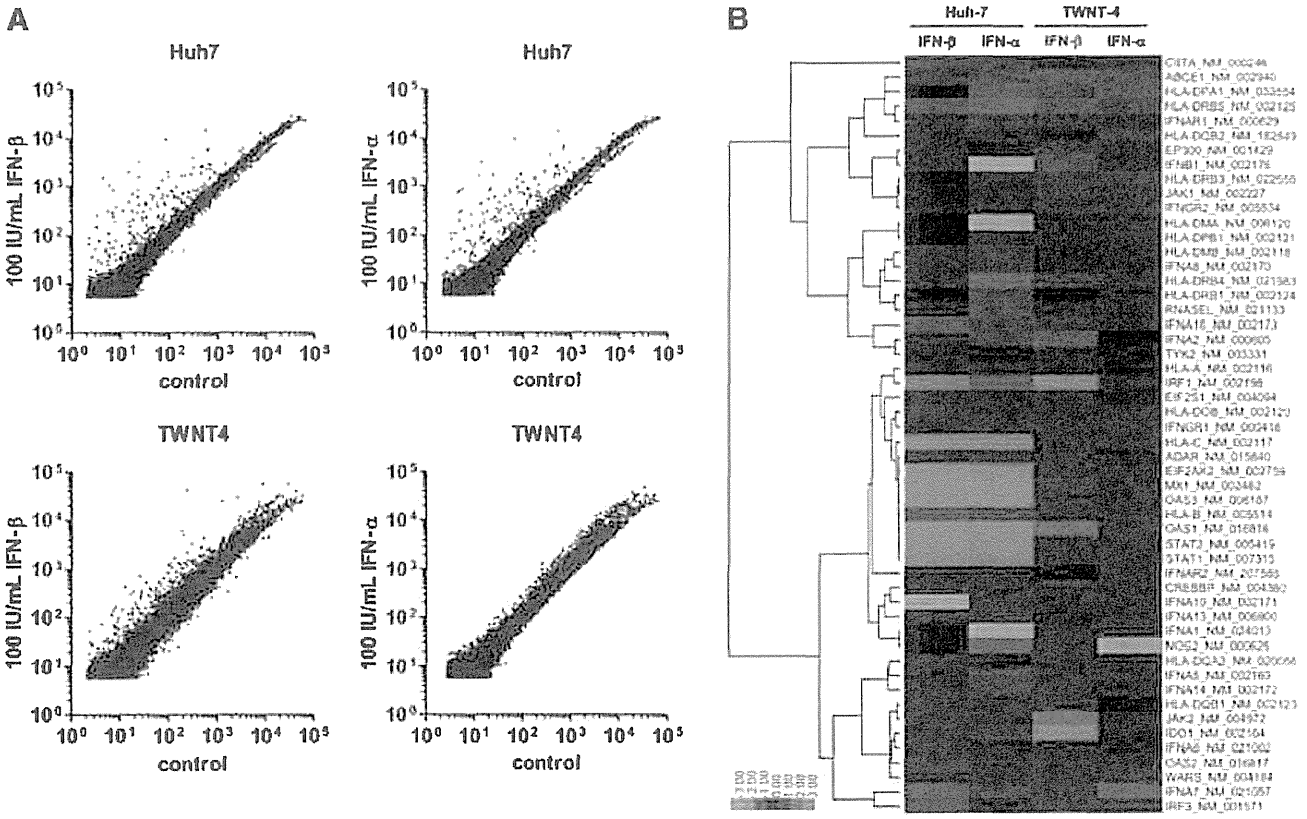

4C ▶

FIG. 2. IFN-induced gene alteration profiles of HSC line or hepatocellular carcinoma cell line. (A) The DNA microarray was hybridized with Cy3 or Cy5-labeled aRNAs, which were extracted from TWNT-4 and HuH-7 cells incubated with IFN-β or IFN-α (100 IU/mL) for 6 h. The scatter plots compare the logarithmic scale (base 2) signal intensities expressed by each gene from microarray experiments. Control indicates nontreated cells. (B) A heat map represents color-coded expression pattern of the gene sets constituting a GeneGo Pathway Map; Antiviral actions of Interferons (Table 1, No. 4), which were constructed by hierarchical cluster analysis using Cluster 3.0 software (http://bonsai.ims.u-tokyo.ac.jp/~mdehoon/software/cluster) and the following graphical analysis using TreeView (http://jtreeview.sourceforge.net/). The *red* or *green* color represents a relatively high or low expression, respectively. HSC, hepatic stellate cell.

TABLE 1. THE STATISTICALLY SIGNIFICANT GENEGO PATHWAY MAPS

No.	GeneGo pathway maps	FDR			
		Huh-7		TWNT-4	
		IFN-β	IFN-α	IFN-β	IFN-α
1	Immune response_IFN alpha/beta signaling pathway	2.87E-05	6.82E-08	5.27E-05	
2	Development_EPO-induced Jak-STAT pathway	1.31E-03	4.54E-04		
3	Immune response_Alternative complement pathway	2.82E-03	2.71E-04		
4	Immune response_Antiviral actions of Interferons		7.79E-04	1.11E-03	
5	Oxidative phosphorylation			1.41E-05	1.87E-13
6	Ligand-independent activation of Androgen receptor in Prostate Cancer			2.71E-04	
7	Cytoskeleton remodeling_TGF, WNT and cytoskeletal remodeling			1.93E-03	
8	Cell adhesion_Plasmin signaling			1.93E-03	
9	Immune response_Role of PKR in stress-induced antiviral cell response			2.87E-05	
10	Immune response_HSP60 and HSP70/TLR signaling pathway			3.25E-05	
11	Immune response_IL-33 signaling pathway			5.27E-05	
12	Immune response_Innate immunte response to RNA viral infection			5.27E-05	
13	Immune response_IL-1 signaling pathway			2.48E-04	
14	Proteolysis_Role of Parkin in the Ubiquitin-Proteasomal Pathway			2.73E-04	
15	Immune response_IL-17 signaling pathways			3.70E-04	
16	Signal transduction_NF-kB activation pathways			4.00E-04	
17	Immune response_TLR2 and TLR4 signaling pathways			5.11E-04	
18	Apoptosis and survival_TNFR1 signaling pathway			5.11E-04	
19	Apoptosis and survival_Role of PKR in stress-induced apoptosis			5.32E-04	
20	Immune response_HMGB1/RAGE signaling pathway			5.32E-04	
21	Development_PEDF signaling			6.35E-04	
22	Neurophysiological process_Receptor-mediated axon growth repulsion			7.51E-04	
23	Immune response_MIF-induced cell adhesion, migration, and angiogenesis			9.19E-04	
24	Immune response_MIF–the neuroendocrine-macrophage connector			9.19E-04	
25	Apoptosis and survival_Apoptotic TNF-family pathways			1.04E-03	
26	Apoptosis and survival_Lymphotoxin-beta receptor signaling			1.04E-03	
27	Immune response_Histamine H1 receptor signaling in immune response			1.25E-03	
28	Immune response_TLR5, TLR7, TLR8, and TLR9 signaling pathways			1.25E-03	
29	Cell cycle_Influence of Ras and Rho proteins on G1/S Transition			1.25E-03	
30	Immune response_Inflammasome in inflammatory response			1.25E-03	
31	Apoptosis and survival_FAS signaling cascades			1.39E-03	
32	Neurophysiological process_Dynein–dynactin motor complex in axonal transport in neurons			1.39E-03	
33	Immune response_Bacterial infections in normal airways			1.39E-03	
34	Cell adhesion_Endothelial cell contacts by junctional mechanisms			1.39E-03	
35	Expression targets of Tissue factor signaling in cancer			1.39E-03	
36	Immune response_MIF-mediated glucocorticoid regulation			1.39E-03	
37	Development_Angiopoietin–Tie2 signaling			1.40E-03	
38	Immune response_IL-18 signaling			1.47E-03	
39	Immune response_MIF in innate immunity response			1.47E-03	
40	Cell adhesion_Ephrin signaling			1.51E-03	
41	Immune response_HMGB1/TLR signaling pathway			1.75E-03	
42	Apoptosis and survival_Caspase cascade			2.96E-03	
43	Development_FGF2-dependent induction of EMT			2.99E-03	
44	Protein folding and maturation_POMC processing				1.07E-12
45	Ubiquinone metabolism				5.45E-06
46	Cytoskeleton remodeling_Regulation of actin cytoskeleton by Rho GTPases				2.38E-05
47	Protein folding and maturation_Insulin processing				4.27E-05
48	Development_Regulation of cytoskeleton proteins in oligodendrocyte differentiation and myelination				1.01E-03

FDR, false discovery rate; IFN, interferon.

3,864 and 2,547 genes in the IFN-β and IFN-α–treated TWNT-4 cells, respectively.

Pathway prediction reveals IFN-β–mediated signaling pathways that are uniquely regulated in TWNT-4 cells

To further characterize the effects of IFN-β and IFN-α on the canonical signaling pathway in both cells, these altered genes were sorted based on gene ontology using GeneGo Pathway Maps, and the statistically significant gene maps (false discovery rate <0.003) are listed in Table 1. They were categorized into common or similar pathways (No. 1–5) and unique pathways (No. 6–48), and the former included an antiviral pathway of IFNs (No. 4). The expression of the gene set constituting No. 4 was examined (Fig. 2B), revealing gene induction patterns almost identical to those in Huh-7 cells. In TWNT-4 cells, there were many quantitative or qualitative differences between IFN-β and IFN-α treatments. While the overall level of gene induction by IFNs tended to be weak, IFN-β altered gene expression levels more dynamically than did IFN-α in HuH-7 cells.

When unique pathways were of interest, of particular note was the fact that there were various unique pathways of IFN-β (No. 9–43) and IFN-α (No. 44–48) identified in TWNT-4 cells. This indicates that each IFN regulates individual signaling pathways in HSCs. Among pathways unique to IFN-β, a pathway with relevance to the cell cycle (No. 29) was identified, in which expression of the p21 gene was increased (1.89-fold) by IFN-β, as well as that of the p21 protein (Fig. 1C). This finding supports the quantitative difference in effects of IFNs on G1 cell cycle arrest in TWNT-4 cells, as demonstrated by flow cytometer analyses (Fig. 1B). Furthermore, many of the pathways unique to IFN-β (No. 9, 10, 17, 19, 20, 24, 30, 33, 39, and 41) were related to common signaling through Toll-like receptor 4 (TLR4), including IFN-β–induced increased expression of the TLR4 gene (2.14-fold), with an associated increase in gene expression of the TLR4 adaptor molecule myeloid differentiation primary response 88 (MyD88), which was also increased (1.84-fold) by IFN-β.

IFN-β exerts histopathological antifibrotic effect in the livers of mice in a NASH model

To provide fundamental information on hepatocellular damage, we performed biochemical liver function tests and confirmed mild elevation of plasma aminotransferase (ALT and AST) levels in CDAA control mice. The mice on a CDAA diet that received IFN-β showed substantially lower levels of ALT and AST, although these changes were not statistically significant (Table 2). On histopathological examination, CDAA control mice, fed a CDAA diet for 8 weeks, exhibited liver fibrosis with occasional bridging between the centrilobular and periportal areas (Fig. 3A, B) and ~4.5-fold augmentation of the area compared with naive mice fed a normal diet (1.45% and 0.32%, respectively) (Fig. 3C). This augmentation was considerably reduced by administration of IFN-β (0.57%), whereas IFN-β did not affect the level of fibrosis in the liver of naive mice (0.29%) (Fig. 3C).

IFN-β downregulates expression of fibrogenic and Myd88 genes in the livers of mice in a NASH model

To investigate the molecular mechanism of IFN-β antifibrotic properties, we examined the levels of expression of genes for fibrogenic mediators, including collagen α1(I) (COL1A1), collagen α1(IV) (COL4A1), and transforming growth factor-β1 (TGF-β1). The expression of all of these genes was elevated in the livers of mice on a CDAA diet compared with naive mice. However, administration of IFN-β significantly attenuated gene expression of COL1A1 and COL4A1 in the livers of mice on a CDAA diet, whereas there was no significant difference in gene expression of TGF-β1 between CDAA control mice and those on a CDAA diet given IFN-β (Fig. 4A–C). Expression of TLR4 and MyD88 genes was also measured to demonstrate the involvement of TLR4 signaling. CDAA control mice showed higher gene expression of both TLR4 and MyD88 in the liver than naive mice, supporting previous studies that used mouse models of NASH (Kawaratani and others 2008; Velayudham and others 2009). In contrast, the level of expression of the MyD88 gene in the livers of mice on a CDAA diet given IFN-β was equal to that of naive mice (Fig. 4E). Lower expression of the TLR4 gene was also observed compared with that in CDAA control mice, although the change was not statistically significant (Fig. 4D). In the livers of naive mice, administration of IFN-β did not affect expression of any fibrogenic gene of interest, whereas there was slight, but significant, upregulation of expression of TLR4 and MyD88 genes (Fig. 4A–E).

Discussion

As HSCs display 2 phenotypes, quiescent and myofibroblastic-activated states, it is important to use cells resembling a phenotype of activated HSCs to evaluate the effects of type I IFNs on hepatic fibrosis *in vitro*. TWNT-4 cells have been reported to exhibit the characteristics of activated HSCs, including fibroblastic morphology and expression of platelet-derived growth factor β receptor, α-SMA, and COL1A1 (Shibata and others 2003). In this study, we demonstrated that IFN-β inhibited TWNT-4 proliferation more potently than IFN-α through G1 cell cycle arrest,

TABLE 2. WEIGHT DATA AND BIOCHEMICAL DATA

Group	N	*Age (week)*	*Body weight (g)*	*Liver wet weight (g)*	*Plasma ALT (IU/L)*	*Plasma AST (IU/L)*
Naive	3	15	24.97±1.42	1.29±0.06	26.0±1.2	64.7±5.3
Naive+IFN-β	3	15	24.75±0.90	1.21±0.05	25.0±1.0	61.7±1.2
CDAA control	5	15	26.25±0.67	1.58±0.07	170.2±17.3	132.0±9.8
CDAA+IFN-β	5	15	26.02±0.91	1.58±0.07	127.6±15.2	108.0±5.1

ALT, alanine aminotransferase; AST, aspartate aminotransferase; CDAA, choline-deficient L-amino acid.

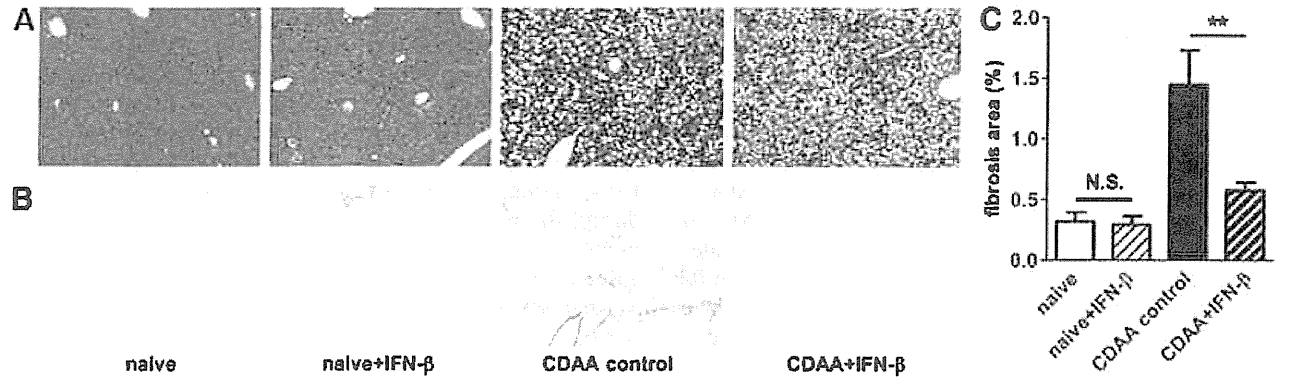

FIG. 3. Antifibrotic efficacy of IFN-β verified by histopathological evaluation of the livers of mice in a NASH model. (A–C) Histopathological evaluation was performed with the livers of mice fed a diet of CRF-1 for 8 weeks (naive), mice on a CRF-1 diet with 4-week administration of IFN-β (naïve+ IFN-β), mice fed a diet of CDAA for 8 weeks (CDAA control), and mice on a CDAA diet with 4-week administration of IFN-β (CDAA+IFN-β). Serial or near-serial sections stained with hematoxylin and eosin (A) and Sirius red (B) (scale bar, 1 mm). (C) Quantitative evaluation of the Sirius red-positive fibrosis area. The results shown represent mean ± S.E.M. ($n=3$–5). $^{**}P<0.01$ between naive versus naive+IFN-β group or CDAA control versus CDAA+IFN-β group (Wilcoxon's test). N.S. means not significant. CDAA, choline-deficient L-amino acid; NASH, nonalcoholic steatohepatitis.

supporting previous studies using rat primary HSCs or other human HSC lines (Shen and others 2002; Sekiya and others 2011). In addition, induction of the p21 protein by IFN-β was detected in TWNT-4 cells, whereas no induction by IFN-α was detected at concentrations up to 1,000 IU/mL, which indicates that TWNT-4 cells are suitable for the investigation of the molecular biological characteristics of IFNs as well as their differences.

For comparative DNA microarray analyses of the effects of type I IFNs on TWNT-4 cells, we selected HuH-7 cells as an appropriate HCC cell line as this has been reported to be more sensitive to IFN-β than IFN-α (Murata and others 2006; Damdinsuren and others 2007). Our DNA microarray analyses revealed that gene expression in TWNT-4 cells was altered more substantially by IFN-β than by IFN-α, and more so than in HuH-7 cells. This finding indicates that HSCs are very sensitive to IFN-β, and that in HSCs, particular pathways are preferentially and selectively modulated by IFN-β. To enhance the credibility of the microarray data, qPCR is useful to independently validate the gene expression changes detected on the microarray. In the case of pathway enrichment analyses conducted in numerous genes, however, qPCR

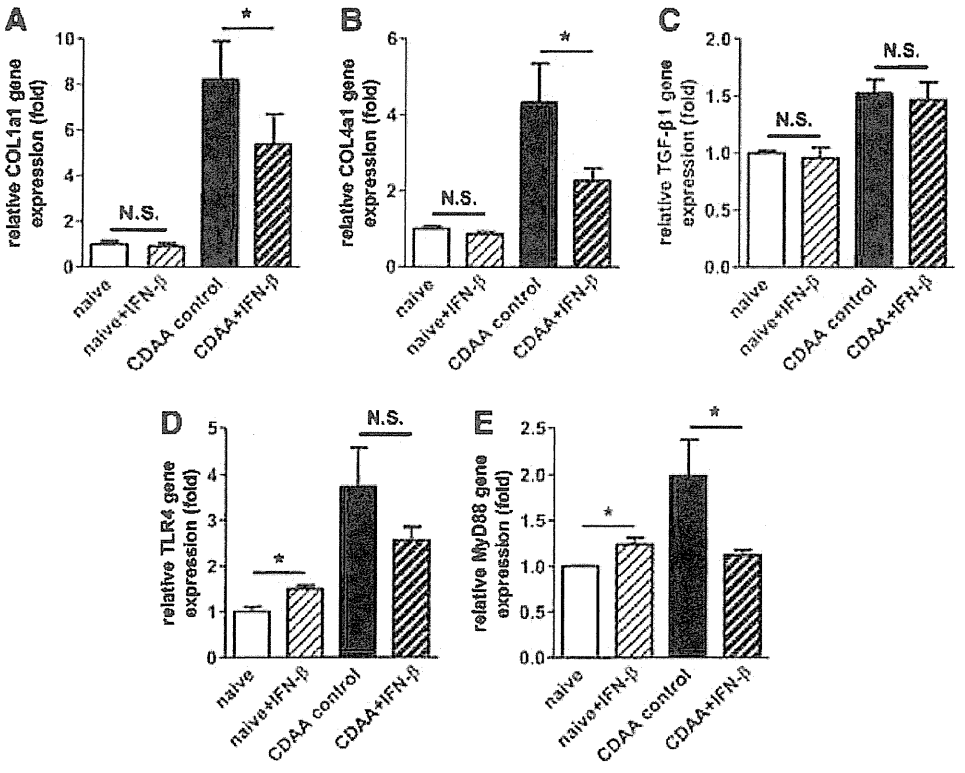

FIG. 4. Transcriptional regulation of fibrogenic and TLR4 signaling-related genes by IFN-β in the livers of mice in a NASH model. Total RNA was isolated from the livers of mice described in the legend of Fig. 3, and then real-time quantitative polymerase chain reaction was performed. The results shown represent the mean ± SEM ($n=3$–5) of the gene expression of COL1A1 (A), COL4A1 (B), TGF-β1 (C), TLR4 (D), and MyD88 (E) relative to those of naive mice. $^{*}P<0.05$ between naive versus naive+IFN-β group or CDAA control versus CDAA+IFN-β group (Wilcoxon's test). N.S. means not significant. TGF-β1, transforming growth factor-β1; TLR4, Toll-like receptor 4.

analysis of each gene expression is basically impractical. Therefore, the transcript abundance of interferon-induced protein with tetratricopeptide repeats 2 (IFIT2), as a representative, was measured using the same RNA samples used on the microarray. It was clearly demonstrated that the IFIT2 gene was differentially expressed by qPCR and had similar SF2 ▶ fold changes to those detected in the microarray (Supplementary Fig. S2). In addition, IFN-β and IFN-α with the same international units of activity would appear to have equivalent antiviral efficacy in HuH-7 cells because of their very similar gene induction pattern of antiviral molecules, which implies that the different gene expression patterns in TWNT-4 cells treated with IFN-β and IFN-α are of significance.

The TLR4 signaling pathway, which is a part of many of the pathways unique to IFN-β–treated TWNT-4 cells, is known to have an important role in regulating fibrogenic responses. A previous study that used HSCs revealed that the TLR4 ligand lipopolysaccharide (LPS) activates inflammatory signals in HSCs through their high expression of TLR4, enhancing HSC activation and fibrosis (Seki and others 2007). Therefore, it is possible that the direct antifibrotic activity of IFN-β is at least partly attributable to modulation of TLR4 signaling in HSCs. Based on this insight, we focused on NASH-related fibrosis to demonstrate the antifibrotic effect of IFN-β using an animal model. The pathogenesis of NASH has not been well understood; however, it can be considered the hepatic manifestation of the metabolic syndrome, and hence NASH is probably the most common cause of hepatic fibrosis worldwide and linked with the increased global prevalence of obesity. Regarding an association between NASH and TLR4 signaling, serum levels of LPS were elevated in NASH patients (Farhadi and others 2008), presumably due to systemic inflammation partly resulting from an overgrowth of gut microflora and increased intestinal permeability (Miele and others 2009).

The CDAA diet-induced mouse model of NASH has been previously demonstrated to represent human NASH by sequentially producing steatohepatitis and liver fibrosis (Denda and others 2002; Kodama and others 2009). Our histopathological examination showed that mice had slight, but significant, fibrosis as a result of being fed a CDAA diet for 8 weeks. Although the feeding period was shorter than that commonly used to validate fibrosis, 20 weeks or more (Denda AU3 ▶ and others 2002; Kodama and others 2010), we believe it was still long enough to allow a satisfactory statistical evaluation of the effect of IFN-β. IFN-β attenuated development of histopathological fibrosis in the CDAA diet-induced mouse model of NASH at a dose of 10^4 IU/body. This is important as it is approximately the same dose used in clinical practice (6×10^6 IU/body), and IFN-β treatment may represent a new therapeutic option for patients with NASH.

It is well known that hepatic injury is largely responsible for the progression of liver fibrosis through accelerated inflammatory responses and follows the activation of HSCs. In this study, the hepatoprotective effect of IFN-β appeared to be absent or weak as manifested by levels of plasma aminotransferases, indicators of hepatocellular damage. Therefore, the detected attenuation of liver fibrosis with IFN-β administration is more likely to result from direct action on HSCs by IFN-β. Meanwhile, given that preventive treatment with IFN-β reduces hepatic injury induced by Con A (Tanabe and others 2007), the possibility remains that the hepatoprotective effect of IFN-β on the NASH model may be detectable using a different regimen. In fact, the preliminary examination had suggested that feeding a CDAA diet for 4 weeks (just before administration of IFN-β in this experimental design) is enough to induce elevation of plasma aminotransferase levels to the plateau phase (unpublished observation) and hence to establish chronic hepatic injury. IFN-β treatment might show a hepatoprotective effect even during the advanced stage of hepatic injury in the NASH model, which would suggest that it probably achieves its antifibrotic effect in an additive manner.

Analyses of fibrogenic gene expression suggest that IFN-β exerts an antifibrotic effect through downregulation of collagen molecules at the transcriptional level. Expression of the TGF-β1 gene did not seem to be affected by IFN-β; in contrast, COL1A1 and COL4A1 have been reported to be common TGF-β1 target genes (Verrecchia and others 2001; Castro and others 2014). These results indicate that IFN-β downregulates fibrogenic gene expression in a TGF-β1–independent manner or that IFN-β modulates protein levels of TGF-β1 in some way. However, the possibility remains that a transient reduction in expression of the TGF-β1 gene was not detected due to the regimen used, in which the liver was removed 3 days after the last administration of IFN-β.

There is considerable evidence that suggests positive regulation of MyD88 by IFN-β in several kinds of cells, including endothelial cells, melanoma cells, and macrophages (da Silva and others 2002; Leaman and others 2003; Thomas and others 2006), supported by the result of our microarray analyses. In addition, *in vivo* induction of hepatic MyD88 gene expression was observed in naive mice as late as 3 days after the last administration of IFN-β. Strikingly, administration of IFN-β to mice with NASH attenuated the gene expression of MyD88 to the naive level, which seems to be at variance with the above-mentioned results. It is possible that these findings might reflect unconventional activity of IFN-β under the pathological condition in liver fibrosis associated with NASH; however, they are more likely due to a decrease in the population of cells with high expression of the MyD88 gene in the liver of mice with NASH. Taking into account that overexpression of MyD88 induces apoptosis (Aliprantis and others 2000), IFN-β might trigger apoptosis when signals of MyD88 exceed a certain threshold through an additive induction on gene expression of MyD88 in the liver of mice with NASH. It is also possible to interpret this finding in light of the antiproliferative effects of IFN-β.

An experimental study using the CDAA diet model showed that MyD88 deficiency protects against NASH-associated liver fibrosis (Miura and others 2010). Another published study indicates that MyD88-deficient HSCs are completely resistant to LPS-mediated downregulation of bone morphogenic protein and activin membrane-bound inhibitor (Bambi), a TGF-β pseudoreceptor (Seki and others 2007). Taking these data into consideration, IFN-β might lead to a situation where only HSCs with low expression of MyD88 remain in the liver of mice with NASH, which promotes efficient induction of Bambi and inhibition of TGF-β–mediated hepatic fibrogenesis. It is particularly noteworthy that our microarray analyses indicated induction activity of IFN-β on the Bambi gene expression in TWNT-4 cells (2.44-fold); for comparison, no increase was detected in IFN-α–treated TWNT-4 cells, IFN-β, and IFN-α–treated HuH-7 cells (1.04-, 0.88-, and 0.86-fold, respectively). To

account for these findings, we propose a bidirectional mechanism of positive regulation of the Bambi gene expression by IFN-β consisting of inhibition of downregulation and induction of upregulation. In this study, we tried to detect both a decrease in gene expression of Bambi, which is thought to occur in HSCs associated with the occurrence of liver fibrosis in mice with NASH, and any recovery effect induced by IFN-β, but found that neither is detectable (unpublished observation). These observations suggest that analysis using whole liver could not identify variation in the expression of Bambi in HSCs. Therefore, further investigations, including cell fractionation analysis, are necessary to confirm whether IFN-β can induce Bambi expression in HSCs of mice with NASH.

Collectively, this study provides the first evidence to show the ability of IFN-β to suppress NASH-related liver fibrosis with accompanying transcriptional downregulation of MyD88. In addition, *in vitro* investigations using TWNT-4 indicate that the antifibrotic activity of IFN-β is attributable to preferential actions on TLR4 signaling and cell proliferation in activated HSCs. Future studies drawing upon the novel findings of this study and taking a closer look at the IFN-β signaling pathway could lead to a potential strategy to improve NASH-related hepatic fibrosis.

Acknowledgments

This work was supported by a grant from the Ministry of Health, Labour and Welfare of Japan to N. Kawada (2008–2010). The authors would like to express their sincere thanks to Dr. Naoya Kobayashi (Okayama Saidaiji Hospital, Okayama, Japan) for his valuable comments regarding this study.

Author Disclosure Statement

No competing financial interests exist.

References

Aliprantis AO, Yang RB, Weiss DS, Godowski P, Zychlinsky A. 2000. The apoptotic signaling pathway activated by Toll-like receptor-2. EMBO J 19(13):3325–3336.

Almasio PL, Venezia G, Craxì A. 2003. The impact of antiviral therapy on the course of chronic HCV infection. A systematic review. Panminerva Med 45(3):175–182.

Bataller R, Brenner DA. 2005. Liver fibrosis. J Clin Invest 115(2):209–218.

Castro NE, Kato M, Park JT, Natarajan R. 2014. Transforming growth factor β1 (TGF-β1) enhances expression of pro-fibrotic genes through a novel signaling cascade and microRNAs in renal mesangial cells. J Biol Chem 289(42):29001–29113.

Damdinsuren B, Nagano H, Wada H, Kondo M, Ota H, Nakamura M, Noda T, Natsag J, Yamamoto H, Doki Y, Umeshita K, Dono K, Nakamori S, Sakon M, Monden M. 2007. Stronger growth-inhibitory effect of interferon (IFN)-beta compared to IFN-alpha is mediated by IFN signaling pathway in hepatocellular carcinoma cells. Int J Oncol 30(1):201–208.

da Silva AJ, Brickelmaier M, Majeau GR, Lukashin AV, Peyman J, Whitty A, Hochman PS. 2002. Comparison of gene expression patterns induced by treatment of human umbilical vein endothelial cells with IFN-alpha 2b vs. IFN-beta 1a: understanding the functional relationship between distinct type I interferons that act through a common receptor. J Interferon Cytokine Res 22(2):173–188.

Denda A, Kitayama W, Kishida H, Murata N, Tsutsumi M, Tsujiuchi T, Nakae D, Konishi Y. 2002. Development of hepatocellular adenomas and carcinomas associated with fibrosis in C57BL/6J male mice given a choline-deficient, L-amino acid-defined diet. Jpn J Cancer Res 93(2): 125–132.

Farhadi A, Gundlapalli S, Shaikh M, Frantzides C, Harrell L, Kwasny MM, Keshavarzian A. 2008. Susceptibility to gut leakiness: a possible mechanism for endotoxaemia in non-alcoholic steatohepatitis. Liver Int 28(7):1026–1033.

Friedman SL, Roll FJ, Boyles J, Bissell DM. 1985. Hepatic lipocytes: the principal collagen-producing cells of normal rat liver. Proc Natl Acad Sci U S A 82(24):8681–8685.

Friedman SL. 2000. Molecular regulation of hepatic fibrosis, an integrated cellular response to tissue injury. J Biol Chem 275(4):2247–2250.

Gäbele E, Brenner DA, Rippe RA. 2003. Liver fibrosis: signals leading to the amplification of the fibrogenic hepatic stellate cell. Front Biosci 8:d69–d77.

Howe PH, Dobrowolski SF, Reddy KB, Stacey DW. 1993. Release from G1 growth arrest by transforming growth factor beta 1 requires cellular ras activity. J Biol Chem 268(28): 21448–21452.

Kawaratani H, Tsujimoto T, Kitazawa T, Kitade M, Yoshiji H, Uemura M, Fukui H. 2008. Innate immune reactivity of the liver in rats fed a choline-deficient L-amino-acid-defined diet. World J Gastroenterol 14(43):6655–6661.

Kodama Y, Kisseleva T, Iwaisako K, Miura K, Taura K, De Minicis S, Osterreicher CH, Schnabl B, Seki E, Brenner DA. 2009. c-Jun N-terminal kinase-1 from hematopoietic cells mediates progression from hepatic steatosis to steatohepatitis and fibrosis in mice. Gastroenterology 137(4):1467–1477.

Leaman DW, Chawla-Sarkar M, Jacobs B, Vyas K, Sun Y, Ozdemir A, Yi T, Williams BR, Borden EC. 2003. Novel growth and death related interferon-stimulated genes (ISGs) in melanoma: greater potency of IFN-beta compared with IFN-alpha2. J Interferon Cytokine Res 23(12):745–756.

Miele L, Valenza V, La Torre G, Montalto M, Cammarota G, Ricci R, Masciana R, Forgione A, Gabrieli ML, Perotti G, Vecchio FM, Rapaccini G, Gasbarrini G, Day CP, Grieco A. 2009. Increased intestinal permeability and tight junction alterations in nonalcoholic fatty liver disease. Hepatology 49(6):1877–1887.

Miura K, Kodama Y, Inokuchi S, Schnabl B, Aoyama T, Ohnishi H, Olefsky JM, Brenner DA, Seki E. 2010. Toll-like receptor 9 promotes steatohepatitis by induction of interleukin-1beta in mice. Gastroenterology 139(1):323–334.

Murakami K, Abe T, Miyazawa M, Yamaguchi M, Masuda T, Matsuura T, Nagamori S, Takeuchi K, Abe K, Kyogoku M. 1995. Establishment of a new human cell line, LI90, exhibiting characteristics of hepatic Ito (fat-storing) cells. Lab Invest 72(6):731–739.

Murata M, Nabeshima S, Kikuchi K, Yamaji K, Furusyo N, Hayashi J. 2006. A comparison of the antitumor effects of interferon-alpha and beta on human hepatocellular carcinoma cell lines. Cytokine 33(3):121–128.

Nagino K, Nomura O, Takii Y, Myomoto A, Ichikawa M, Nakamura F, Higasa M, Akiyama H, Nobumasa H, Shiojima S, Tsujimoto G. 2006. Ultrasensitive DNA chip: gene expression profile analysis without RNA amplification. J Biochem 139(4):697–703.

Nakabayashi H, Taketa K, Miyano K, Yamane T, Sato J. 1982. Growth of human hepatoma cells lines with differentiated functions in chemically defined medium. Cancer Res 42(9): 3858–3863.

Pestka S, Langer JA, Zoon KC, Samuel CE. 1987. Interferons and their actions. Annu Rev Biochem 56:727–777.

Seki E, De Minicis S, Osterreicher CH, Kluwe J, Osawa Y, Brenner DA, Schwabe RF. 2007. TLR4 enhances TGF-beta signaling and hepatic fibrosis. Nat Med 13(11):1324–1332.

Sekiya Y, Ogawa T, Iizuka M, Yoshizato K, Ikeda K, Kawada N. 2011. Down-regulation of cyclin E1 expression by microRNA-195 accounts for interferon-β-induced inhibition of hepatic stellate cell proliferation. J Cell Physiol 226(10): 2535–2542.

Shen H, Zhang M, Minuk GY, Gong Y. 2002. Different effects of rat interferon alpha, beta and gamma on rat hepatic stellate cell proliferation and activation. BMC Cell Biol 3:9.

Shibata N, Watanabe T, Okitsu T, Sakaguchi M, Takesue M, Kunieda T, Omoto K, Yamamoto S, Tanaka N, Kobayashi N. 2003. Establishment of an immortalized human hepatic stellate cell line to develop antifibrotic therapies. Cell Transplant 12(5):499–507.

Soga K, Shibasaki K, Aoyagi Y. 2005. Effect of interferon on incidence of hepatocellular carcinoma in patients with chronic hepatitis C. Hepatogastroenterology 52(64):1154–1158.

Tanabe J, Izawa A, Takemi N, Miyauchi Y, Torii Y, Tsuchiyama H, Suzuki T, Sone S, Ando K. 2007. Interferon-beta reduces the mouse liver fibrosis induced by repeated administration of concanavalin A via the direct and indirect effects. Immunology 122(4):562–570.

Thomas KE, Galligan CL, Newman RD, Fish EN, Vogel SN. 2006. Contribution of interferon-beta to the murine macrophage response to the toll-like receptor 4 agonist, lipopolysaccharide. J Biol Chem 281(41):31119–31130.

Velayudham A, Dolganiuc A, Ellis M, Petrasek J, Kodys K, Mandrekar P, Szabo G. 2009. VSL#3 probiotic treatment attenuates fibrosis without changes in steatohepatitis in a diet-induced nonalcoholic steatohepatitis model in mice. Hepatology 49(3):989–997.

Verrecchia F, Chu ML, Mauviel A. 2001. Identification of novel TGF-beta/Smad gene targets in dermal fibroblasts using a combined cDNA microarray/promoter transactivation approach. J Biol Chem 276(20):17058–17062.

Address correspondence to:
Rieko Shimozono ◀AU5
Pharmaceutical Research Laboratory
Toray Industries, Inc.
6-10-1, Tebiro
Kamakura
Kanagawa 248-8555
Japan

E-mail: rieko_shimozono@nts.toray.co.jp

Received 7 June 2014/Accepted 13 December 2014

Supplementary Data

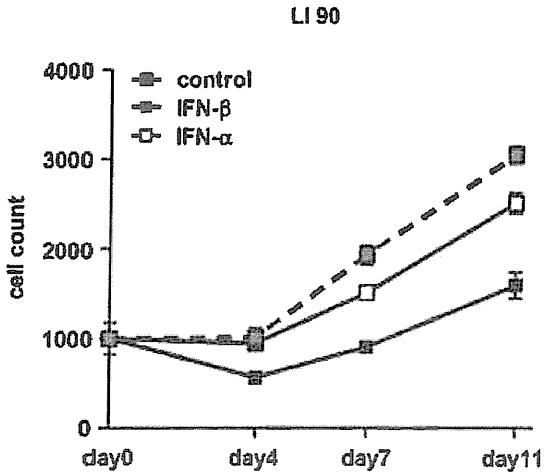

SUPPLEMENTARY FIG. S1. Antiproliferative effects of IFNs on LI 90 cells. LI 90 cells (JCRB0160) obtained from the Japanese Collection of Research Bioresources were incubated with IFN-β or IFN-α (100 IU/mL) for 4–11 days. The IFN-containing medium was replaced every 4 days. Viable cell count was determined by MTS methods. Cell growth is shown as a percentage when the average cell number for control cells without IFNs was arbitrarily set to 100% and that for seeded cells on day 0 was arbitrarily set to 0%. The results shown represent the mean ± SD from triplicate-quintuplicate assays. Control indicates nontreated cells. IFN, interferon.

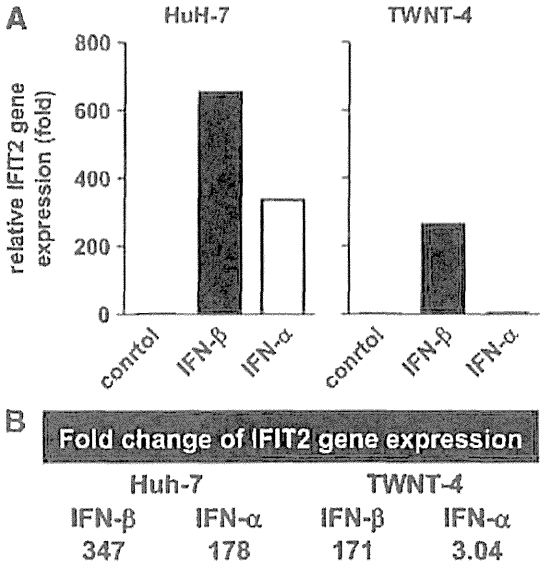

B

Fold change of IFIT2 gene expression			
Huh-7		TWNT-4	
IFN-β	IFN-α	IFN-β	IFN-α
347	178	171	3.04

SUPPLEMENTARY FIG. S2. IFN-induced upregulation of IFIT2 gene expression in HuH-7 cells or TWNT-4 cells. (A) The RNA samples used on the microarray were translated into cDNA, then each cDNA was subjected to real-time quantitative polymerase chain reaction using the gene-specific primers for the IFIT2 gene (forward: 5′-TGGTGGC AGAAGAGGAAGAT-3′, reverse: 5′-CCAAGGAATTCTT ATTGTTCTCACT-3′) and the glyceraldehyde-3-phosphate dehydrogenase (GAPDH) gene (forward: 5′-TGATGACAT CAAGAAGGTGGTGAAG-3′, reverse: 5′-ATGGCCTACA TGGCCTCCAAGGA-3′). The relative amounts of the IFIT2 gene were determined using the $2^{-\Delta\Delta CT}$ method. The cycle threshold (Ct) values of the IFIT2 gene were corrected against values for the reference gene GAPDH (ΔCt) and normalized against the ΔCt of the control sample (ΔΔCt). Control indicates nontreated cells. (B) IFN-induced fold changes for the IFIT2 gene in the microarray analysis. cDNA, complementary DNA; IFIT2, interferon-induced protein with tetratricopeptide repeats 2.

SUPPLEMENTARY TABLE S1. NUCLEOTIDE SEQUENCE OF PRIMERS FOR THE REAL-TIME QUANTITATIVE PCR ANALYSIS

Name	Species	Primer Sequence	
		Forward	Reverse
COL1A1	Mouse	5'-tggaagagcggagagtactg-3'	5'-gtactcgaacgggaatccat-3'
COL4A1	Mouse	5'-ggtgtcagcaattaggcaggtcaag-3'	5'-actccacgcagagcagaagcaagaa-3'
TGF-β1	Mouse	5'-aacaacgccatctatgag-3'	5'-tattccgtctccttggtt-3'
TLR4	Mouse	5'-ggactctgatcatggcactg-3'	5'-ctgatccatgcattggtaggt-3'
MyD88	Mouse	5'-gccttgttagaccgtgaggat-3'	5'-ctaagtatttctggcagtcctcct-3'
GAPDH	Mouse	5'-tgatgacatcaagaaggtggtgaag-3'	5'-atggcctacatggcctccaagga-3'

AUTHOR QUERY FOR JIR-2014-0096-VER9-SHIMOZONO_1P

AU1: Please note that gene symbols in any article should be formatted as per the gene nomenclature. Thus, please make sure that gene symbols, if any in this article, are italicized.
AU2: Please review all authors' surnames for accurate indexing citations.
AU3: "Uzé and others 2007" and "Kodama and others 2010" are cited in the text, but not found in the reference list. Please check.
AU4: Please expand α-SMA.
AU5: Please mention the academic title of the corresponding author.

Laboratory Investigation (2015) 95, 515–524

Involvement of hepatic stellate cell cytoglobin in acute hepatocyte damage through the regulation of CYP2E1-mediated xenobiotic metabolism

Yuga Teranishi[1,5], Tsutomu Matsubara[2,5], Kristopher W Krausz[3], Thi TT Le[1], Frank J Gonzalez[3], Katsutoshi Yoshizato[1,4], Kazuo Ikeda[2] and Norifumi Kawada[1]

Oxygen (O_2) is required for cytochrome P450 (CYP)-dependent drug metabolism. Cytoglobin (CYGB) is a unique globin expressed exclusively in hepatic stellate cells (HSCs). However, its role in O_2-dependent metabolism in neighboring hepatocytes remains unknown. This study provides evidence that CYGB in HSCs is involved in acetaminophen (*N*-acetyl-*p*-aminophenol; APAP)-induced hepatotoxicity. Serum alanine aminotransferase levels were higher in wild-type mice than in *Cygb*-null mice. Wild-type mice exhibited more severe hepatocyte necrosis around the central vein area compared with *Cygb*-null mice, thus indicating that CYGB deficiency protects against APAP-induced liver damage. Although no difference in the hepatic expression of CYP2E1, a key enzyme involved in APAP toxicity, was observed between wild-type and *Cygb*-null mice, the serum levels of the APAP metabolites cysteinyl-APAP and *N*-acetyl-cysteinyl-APAP were decreased in *Cygb*-null mice, suggesting reduced APAP metabolism in the livers of *Cygb*-null mice. In primary cultures, APAP-induced hepatocyte damage was increased by co-culturing with wild-type HSCs but not with *Cygb*-null HSCs. In addition, cell damage was markedly alleviated under low O_2 condition (5% O_2), suggesting the requirement of O_2 for APAP toxicity. Carbon tetrachloride-induced liver injury (CYP2E1-dependent), but not lipopolysaccharide/D-galactosamine-induced injury (CYP2E1-independent), was similarly alleviated in *Cygb*-null mice. Considering the function of CYGB as O_2 carrier, these results strongly support the hypothesis that HSCs are involved in the CYP2E1-mediated xenobiotic activation by augmenting O_2 supply to hepatocytes. In conclusion, CYGB in HSCs contributes to the CYP-mediated metabolism of xenobiotics in hepatocytes by supplying O_2 for enzymatic oxidation.
Laboratory Investigation (2015) **95,** 515–524; doi:10.1038/labinvest.2015.29; published online 16 February 2015

The metabolism of xenobiotics, including clinical drugs, occurs primarily in the liver. Most xenobiotic detoxification metabolism involves cytochrome P450 (CYP) enzymes, which are predominantly expressed in the liver,[1] and these processes occasionally result in acute hepatocyte damage. For instance, acetaminophen (*N*-acetyl-*p*-aminophenol; APAP) and carbon tetrachloride (CCl_4) are metabolized by CYP to generate toxic intermediates.

APAP is commonly used as an antipyretic and analgesic drug. CYP-mediated APAP metabolism is known to generate *N*-acetyl-*p*-benzoquinone imine (NAPQI), which binds to cellular macromolecules and initiates hepatocyte damage if present at high concentrations under glutathione (GSH) depletion.[2] CYP1A2, CYP2A6, CYP2E1, and CYP3A have been identified as enzymes that generate NAPQI from APAP.[3] Among these CYPs, CYP2E1 has the lowest K_m for APAP, and the CYP2E1-dependent metabolism of APAP can result in hepatotoxicity.[4] CYP2E1 is a monooxygenase that requires molecular oxygen (O_2) for its enzymatic activity. A recent study reported that the APAP-induced damage to primary mouse hepatocytes was reduced under a low O_2 concentration (5% O_2) compared with normoxic conditions (20% O_2).[5] Thus, APAP-induced acute liver injury may be dependent on hepatic O_2 levels.

The aerobic metabolism of mammals relies on respiratory proteins that function in the transport and storage of O_2.

[1]Department of Hepatology, Graduate School of Medicine, Osaka City University, Osaka, Japan; [2]Department of Anatomy and Regenerative Biology, Graduate School of Medicine, Osaka City University, Osaka, Japan; [3]Laboratory of Metabolism, Center for Cancer Research, National Cancer Institute, National Institutes of Health, Bethesda, MD, USA and [4]Phoenixbio Co., Ltd, Hiroshima, Japan
Correspondence: Professor N Kawada, MD, PhD, Department of Hepatology, Graduate School of Medicine, Osaka City University, 1-4-3, Asahimachi, Abeno, Osaka 545-8585, Japan.
E-mail: kawadanori@med.osaka-cu.ac.jp
[5]These authors contributed equally to this work.

Received 20 June 2014; revised 30 October 2014; accepted 21 November 2014

Four globin proteins are known to contribute to O_2 homeostasis in mammals.[6,7] Hemoglobin in erythrocytes has an important role in the transport of O_2 from the bloodstream to the viscera. In the viscera, myoglobin, neuroglobin, and cytoglobin (CYGB) act as local O_2-binding molecules that facilitate the intracellular diffusion of O_2.[8] Notably, CYGB in mammals is expressed in various organs, including the liver, heart, brain, and the lung. CYGB is a hexacoordinated heme-containing protein that is able to bind O_2, nitric oxide, and carbon monoxide.[9,10] CYGB expression increases in response to the duration and severity of hypoxia.[11] Thus, CYGB is thought to be an O_2 sensor for the local storage and transport of O_2; however, its contribution to O_2-dependent xenobiotic metabolism remains unclear.

CYGB is a unique globin expressed exclusively in hepatic stellate cells (HSCs), which represent ~5–8% of the cells in the liver.[12] When liver injury occurs, HSCs undergo activation and acquire myofibroblastic characteristics, including increased collagen production. Such characteristic alterations of HSCs are believed to be strongly associated with hepatic fibrosis and the development of liver cirrhosis and cancer. In addition, interactions between hepatocytes and HSCs, as well as the involvement of HSCs in hepatic tissue growth and regeneration have been reported.[13,14] However, the interplay between HSCs and hepatocytes in drug metabolism remains uncharacterized. Furthermore, the effect of CYGB in HSCs (HSC-CYGB) on APAP-induced acute liver injury has never been investigated.

In this study, the correlation between HSC-CYGB and xenobiotic-mediated hepatocyte injury was investigated *in vivo* and *in vitro* using *Cygb*-null mice. The results implied that a CYGB deficiency in HSCs can regulate hepatic O_2 levels and can alleviate the acute liver injury induced by APAP and CCl_4, by decelerating CYP2E1 metabolism in hepatocytes.

MATERIALS AND METHODS

Materials

All reagents were obtained from Sigma-Aldrich (St Louis, MO, USA) or Wako Pure Chemical (Osaka, Japan), unless otherwise noted.

Mouse Studies

Eight- to 12-week-old male C57BL/6 mice were purchased from Japan SLC (Shizuoka, Japan). *Cygb*-null mice were generated in our laboratory as previously described.[15] *Cygb*-null mice were compared with their wild-type littermates. All mice were cared for according to the guidelines approved by the Institutional Animal Care and Use Committee of Osaka City University, Osaka, Japan. Before APAP treatment, the mice were fasted for 16 h. APAP dissolved in isotonic saline at 65 °C was intraperitoneally (i.p.) injected (300 mg/kg) into mice, which were killed 6 h later. In the study of CCl_4-induced acute liver injury, mice were i.p. injected with CCl_4 (0.5 mg/kg) suspended in corn oil, fasted, and killed 24 h after the injection. Another group of mice were administered D-galactosamine (D-GalN; 700 mg/kg) and lipopolysaccharide (LPS; 5 μg/kg, *Escherichia coli* 0111:B4) suspended in saline and were killed 6 h later. Blood and liver tissues were collected and stored at −80 °C for subsequent analysis. For histopathological analysis, small pieces of the liver were fixed in 4% formaldehyde overnight and embedded in paraffin. The liver tissue was sectioned at 5-μm thickness and stained with hematoxylin and eosin. Relative necrotic area (%) was estimated by using Image J software.

Isolation, Fractionation, and Culture of Liver Cells

Hepatocytes and HSCs were isolated from male C57BL/6 mice as previously described.[16] APAP (2.5, 5, 10, 20, or 30 mM) was dissolved in William's Medium E (Gibco, Grand Island, NY) at 65 °C. Hepatocytes were plated in 12- or 24-well plates (1×10^5 cells/ml) (Celltight C-1 Collagen-I, Sumitomo Bakelite, Tokyo, Japan) and were pre-incubated in William's Medium E supplemented with 10% fetal bovine serum (Gibco) and 0.1 μM dexamethasone for 3 h before APAP treatment. For co-culture experiments, HSCs (5×10^5 cells/well) were plated in cell culture inserts (Transparent PET membrane, 1.0 μm pore size; Corning, Corning, NY, USA) and incubated overnight in the William's Medium E before co-culture with hepatocytes. The cells were incubated for 16 h with APAP-containing media under a 5% or 20% O_2 atmosphere. Conditioned media derived from the 16-h culture of wild-type or *Cygb*-null HSCs were also used.

Measurement of ALT Activity and APAP Metabolites in Serum

Serum alanine aminotransferase (ALT) activity was determined using a kinetic test (SRL, Tokyo, Japan). The levels of APAP and its metabolites in sera collected 2 h after APAP injection were quantified as previously reported.[4]

Visualization of Hypoxia With Pimonidazole

Mice were injected with APAP (300 mg/kg, i.p.), followed by the administration of pimonidazole hydrochloride (60 mg/kg, i.p.; Hypoxyprobe, Burlington, MA, USA) 1 h before being killed. Small liver pieces were fixed in 4% paraformaldehyde and embedded in paraffin. Paraffin sections (5 μm) were prepared in the Central Laboratory of the Osaka City University Medical School. Pimonidazole was detected using a Hypoxyprobe-1 Plus Kit, according to the manufacturer's instructions. An anti-fluorescein antibody conjugated to Texas Red (Ab6654; Abcam, Cambridge, UK) was used to visualize the reaction.

GSH Measurements

Liver tissues (100 mg) were homogenized in 1 ml of ice-cold phosphate-buffered saline containing 1 mM EDTA (pH 7.5) and were centrifuged at 10 500 *g* for 15 min at 4 °C. The supernatants were collected and the GSH content in each

sample was determined using a GSH quantification kit (Dojindo, Kumamoto, Japan).

Quantitative Real-Time Reverse Transcription-PCR Analyses

Total RNA was isolated using TRIzol reagent (Invitrogen, Carlsbad, CA). cDNA was generated with random hexamer primers (Invitrogen) and the SuperScript RT II enzyme (Invitrogen). Quantitative PCRs were performed using the ABI 5500 Real-Time PCR System (Applied Biosystems, Foster City, CA, USA). The primers used are listed in Supplementary Table 1. Relative expression levels were calculated using the comparative CT method. The expression levels were normalized to that of 18S ribosomal RNA.

Western Blotting

Liver tissues were homogenized with RIPA buffer (50 mM Tris-HCl pH 8.0, 150 mM NaCl, 1% Triton X-100, 1% SDS) containing a protease inhibitor (Roche, Basel, Switzerland) and phosphatase inhibitors (1 mM sodium fluoride, 1 mM β-glycerol phosphate, and 1 mM sodium vanadate) and were centrifuged at 10 000 *g* for 10 min. The supernatants (25 μg protein) were subjected to western blot analysis of CYP2E1. To obtain nuclear extracts, liver tissues were prepared using the NE-PER Nuclear and Cytoplasmic Extraction Reagents kit (Thermo Fisher Scientific, Waltham, MA), according to the manufacturer's protocol. The nuclear extracts (20 μg protein) were subjected to western blot analysis of HIF-1α. Primary hepatocytes, cultured under a hypoxic conditions (1% O_2), were used as positive control (5 μg) for western blotting of HIF-1α. The samples were separated on SDS-polyacrylamide gels and transferred to polyvinylidene fluoride membranes using standard western blotting techniques. The membranes were incubated with an antibody against CYP2E1 (kindly provided by Dr Koichi Yoshinari (Tohoku University, Sendai, Japan)) at a dilution of 1:10 000 or with an antibody against HIF-1α (NB100-449, Novus Biologicals, Littleton, CO) at a dilution of 1:1000. The CYP2E1 protein levels in the samples were normalized to those obtained with a glyceraldehyde-3-phosphate dehydrogenase antibody at a dilution of 1:10 000 (MAB374; Millipore, Billerica, MA, USA). The expression of HIF-1α was normalized to the signal obtained with Coomassie brilliant blue staining.

Measurement of Hepatic CYP2E1 Activity *In Vitro*

Liver tissues (100 mg) were homogenized in 1 ml of ice-cold 50 mM potassium phosphate buffer (pH 7.4). The homogenate was centrifuged at 9000 *g* for 20 min. The supernatant was transferred to a new tube and centrifuged at 105 000 *g* for 60 min. The pellet was suspended with 50 mM Tris-HCl (pH 7.4)/20% glycerol. The suspension was subjected to CYP2E1 activity assay with vivid CYP2E1 blue screening kit (Invitrogen).

Assessment of Cell Death and Viability in Primary-Cultured Mouse Hepatocytes

Cell death was analyzed with 1 μg/ml propidium iodide (Dojindo), which stains nuclei only when the cellular plasma membranes become permeabilized, and with Hoechst 33342 (Dojindo). Cell viability was determined using an MTT assay.[17] The cell viability (%) of the test samples was calculated relative to that of the control sample.

Statistical Analysis

The statistical analysis was performed using Prism version 6.0 software (GraphPad Software, San Diego, CA, USA). A *P*-value <0.05 was considered to indicate a significant difference.

RESULTS

Alleviation of APAP-Induced Liver Injury in *Cygb*-Null Mice

A single injection of APAP (300 mg/kg, i.p.) into C57Bl/6 mice induced significant liver injury, which was accompanied by a marked increase in the serum ALT levels (Supplementary Figure S1A) and a moderate to marked centrilobular necrosis (Supplementary Figure S1B) 6–12 h after the injection. Thus, in the subsequent experiments, wild-type and *Cygb*-null mice were killed 6 h after APAP injection.

The increase in serum ALT levels was significantly attenuated in the *Cygb*-null mice receiving APAP: the ALT levels of the wild-type and *Cygb*-null mice were 13 970 ± 2370 and 4699 ± 1226 U/l, respectively (Figure 1a). In accordance with these results, the histological area of hepatocyte necrosis was diminished in the *Cygb*-null mice (Figure 1b). Relative necrotic area was larger in wild-type (47.3 ± 11.0%) than in *Cygb*-null mice (17.8 ± 5.0%) as shown in Figure1c. The APAP-induced increase in the hepatic mRNA levels of chemokine (C–C motif) ligand 2 (*Ccl2*) in the *Cygb*-null mice was reduced to half of that detected in the wild-type mice. No differences in the hepatic mRNA expression levels of tumor necrosis factor α, interleukin 1β, or interleukin 6 were observed between the wild-type and *Cygb*-null mice (Figure 1d). Hepatic GSH level in both mouse lines decreased dramatically at 2 h after APAP challenge. After the maximum depletion, hepatic GSH level in *Cygb*-null mice recovered quickly, compared with that in wild-type mice (Figure 1e). Three of the tested five wild-type mice showed low hepatic GSH level at 6 h after APAP injection, compared with *Cygb*-null mice (Figure 1f). Taken together, these results suggest that CYGB deficiency restrained APAP-induced acute liver injury.

Reduced Serum APAP Metabolites and Lower Hepatic O_2 Levels in *Cygb*-Null Mice

The hepatic expression of CYP2E1, an enzyme that generates NAPQI from APAP, was investigated in wild-type and *Cygb*-null mice. We confirmed previous reports indicating that hepatic CYP2E1 mRNA levels decreased in a

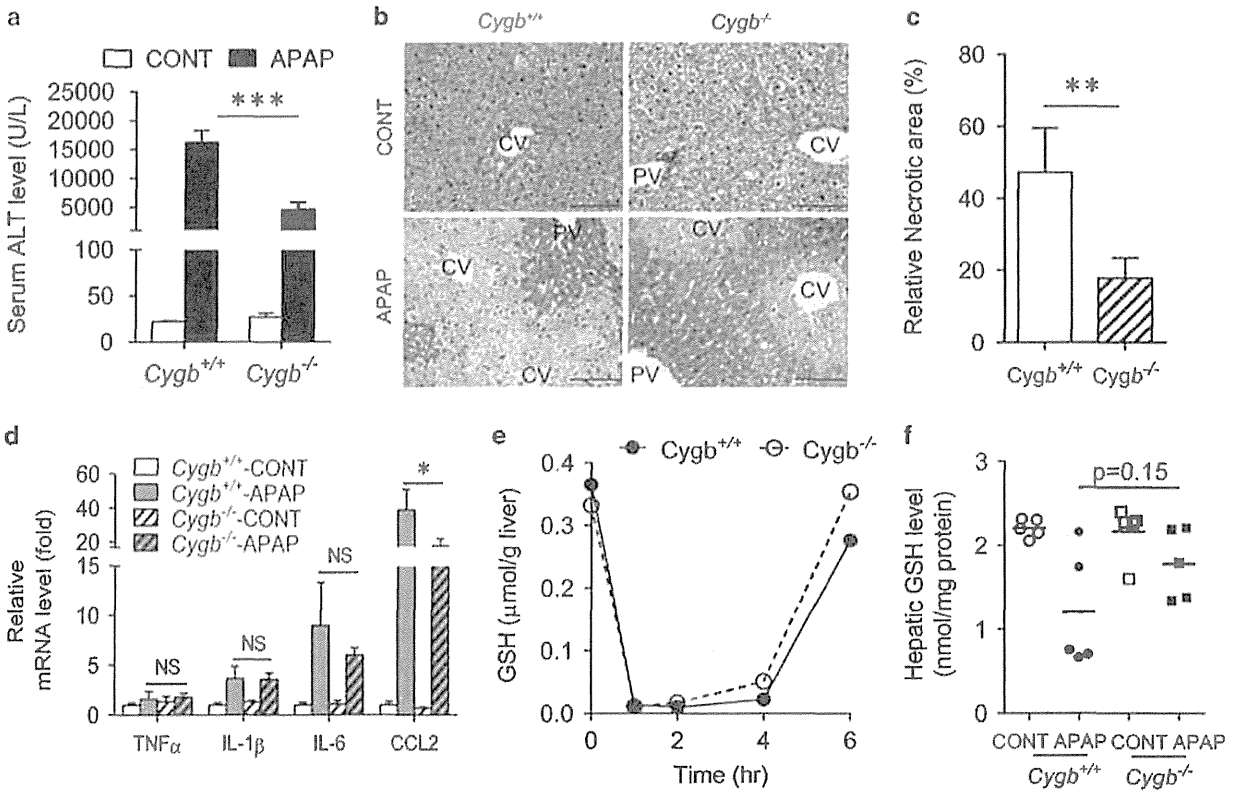

Figure 1 Analysis of *N*-acetyl-*p*-aminophenol (APAP)-induced acute liver injury in wild-type and cytoglobin (*Cygb*)-null mice. (**a**) Serum alanine aminotransferase (ALT) levels. ALT activity was measured 6 h after saline (CONT) or 300 mg/kg APAP administration. Each bar represents the mean value and s.d. ($n=5$–6). (**b**) Representative liver sections stained with hematoxylin and eosin (× 400, bar = 100 μm). CV, central vein. PV, portal vein. (**c**) Relative necrotic area was represented by the percentage ratio of necrotic area to liver area. Each bar represents the mean value and s.d. ($n=5$). (**d**) Quantitative reverse transcription-PCR analysis of tumor necrosis factor-α (*TNF-α*), interleukin (*IL*)-*1β*, *IL-6*, and chemokine (C–C motif) ligand 2 (*Ccl2*) mRNAs during APAP-induced liver injury. Each bar represents the mean value and s.d. ($n=5$–6). (**e**) Time course of glutathione (GSH) levels in the liver ($n=2$). (**f**) Hepatic GSH level at 6 h. Each bar represents the mean value ($n=5$). Wild-type and *Cygb*-null mice are designated $Cygb^{+/+}$ and $Cygb^{-/-}$, respectively. Significance was determined by a one-way ANOVA with Bonferroni's test. $^{*}P<0.05$, $^{***}P<0.001$; NS, not significant.

time-dependent manner after APAP injection in wild-type mice (Supplementary Figure S1C).[18] No differences were noted in the CYP2E1 mRNA and protein levels between untreated wild-type and *Cygb*-null mice (Figures 2a and b). After APAP challenge, similar decreases in the CYP2E1 mRNA and protein levels were observed in the wild-type and *Cygb*-null mice. Furthermore, the hepatic microsomal CYP2E1 activity *in vitro* was assessed. The Michaelis–Menten kinetics curve for the CYP2E1 activity of *Cygb*-null mice were almost same to that for the wild-type mice. In addition, the V_{max} and the K_m were 0.325 ± 0.10 nmol per mg protein/min and 17.48 ± 9.85 μM for the wild-type mice, and 0.338 ± 0.03 nmolper mg protein/min and 19.72 ± 2.58 μM for the *Cygb*-null mice, respectively. The differences between the wild-type and the *Cygb*-null mice were not observed (Figure 2c). However, the serum levels of CYP2E1-dependent APAP metabolites, ie, cysteinyl-APAP and *N*-acetyl-cysteinyl-APAP, which are derived from NAPQI (Figure 2d), were significantly decreased in the *Cygb*-null mice compared with the wild-type mice. In contrast, the APAP levels tended to be high in the *Cygb*-null mice and the levels of APAP-glucuronide, a CYP2E1-independent metabolite, remained unchanged (Figure 2e).

As O_2 is required for the CYP2E1-mediated NAPQI generation, we hypothesized that the livers of the *Cygb*-null mice had low concentrations of O_2 compared with the wild-type mice. To test this hypothesis, pimonidazole was used, which is frequently used to detect hypoxic regions in tissues.[19] The resulting pimonidazole staining was limitedly positive around the central vein of the untreated livers. However, after treatment with APAP for 6 h, the pimonidazole-positive areas expanded to zone 2 (intermediate area) in the livers of the *Cygb*-null mice, but not in the wild-type mice (Figure 3a). Although HIF-1α protein was not detected (Figure 3b), the data may support that CYGB deficiency results in decreased hepatic O_2 levels after APAP challenge.

Attenuation of APAP-Induced Cell Death in Primary-Cultured Mouse Hepatocytes by Hypoxia

Cultured primary mouse hepatocytes were challenged with 2.5–20 mM APAP under 5 or 20% O_2 for 16 h. The APAP

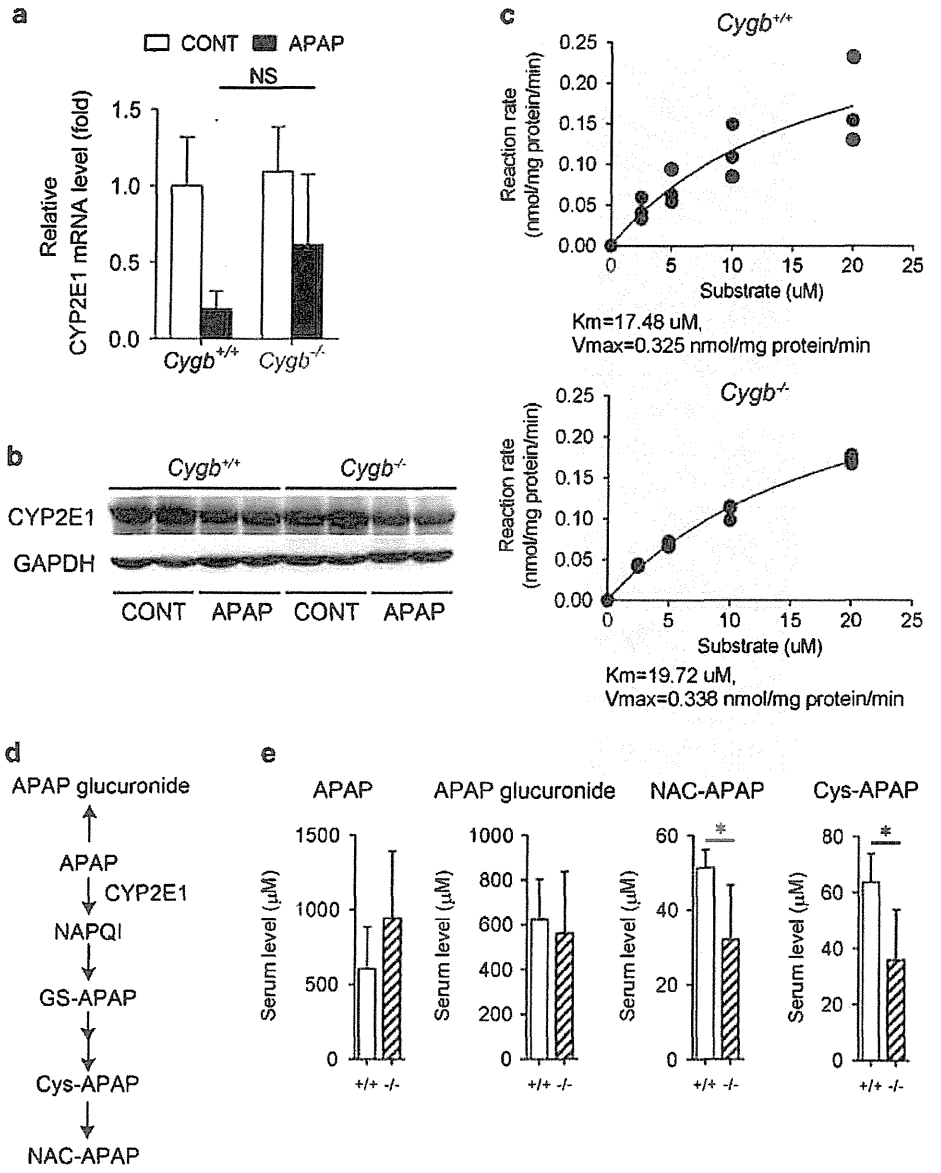

Figure 2 Cytochrome P450, family 2, subfamily E, polypeptide 1 (CYP2E1) expression and *N*-acetyl-*p*-aminophenol (APAP) metabolism in the liver. Quantitative reverse transcription-PCR (**a**) and western blot (**b**) analyses of CYP2E1 expression in the liver 6 h after APAP. Each bar represents the mean value and s.d. ($n = 5$–6). Significance was determined by a one-way ANOVA with Bonferroni's test (NS, not significant). (**c**) Major *in vivo* APAP metabolic pathways are indicated. GS-APAP, 3-gultathionyl-APAP; Cys-APAP, cysteinyl-APAP; NAC-APAP, *N*-acetyl-cysteinyl-APAP. (**d**) Serum levels of APAP and its major metabolites in *Cygb*$^{+/+}$ and *Cygb*$^{-/-}$ mice. Serum samples were collected 2 h after the administration of APAP, and APAP metabolites were measured by a liquid chromatography-mass spectrometry (LC-MS) analysis. The values are expressed as the relative abundance (mean and s.d., $n = 5$). Significance was determined using an unpaired *t*-test (*$P < 0.05$). (**e**) Hepatic microsomal CYP2E1 activity. The reaction rate was determined as described in Materials and Methods.

challenge induced cell death in a dose-dependent manner under 20% O_2. Notably, the hepatocyte damage was significantly greater under 20% O_2 than under 5% O_2: when cells were treated with 20 mM APAP, the hepatocyte death in the presence of 20 and 5% O_2 was 67.0 and 31.8%, respectively (Figures 4a and b). In accordance with these results, cell viability after exposure to APAP was lower in the presence of 20% O_2 than in the presence of 5% O_2 (Figure 4c). HIF-1α protein was detected in the presence of 1% O_2, but not in the presence of 5 and 20% O_2 (Figure 4d). These results demonstrated that the O_2 concentration influences the APAP toxicity in primary-cultured hepatocytes without HIF1α activation.